Three-Dimensional Structure of Poliovirus at 2.9 Å Resolution

J. M. Hogle, M. Chow, D. J. Filman

Abstract. *The three-dimensional structure of poliovirus has been determined at 2.9 Å resolution by x-ray crystallographic methods. Each of the three major capsid proteins (VP1, VP2, and VP3) contains a "core" consisting of an eight-stranded antiparallel beta barrel with two flanking helices. The arrangement of beta strands and helices is structurally similar and topologically identical to the folding pattern of the capsid proteins of several icosahedral plant viruses. In each of the major capsid proteins, the "connecting loops" and NH_2- and COOH-terminal extensions are structurally dissimilar. The packing of the subunit "cores" to form the virion shell is reminiscent of the packing in the* T = 3 *plant viruses, but is significantly different in detail. Differences in the orientations of the subunits cause dissimilar contacts at protein-protein interfaces, and are also responsible for two major surface features of the poliovirion: prominent peaks at the fivefold and threefold axes of the particle. The positions and interactions of the NH_2- and COOH-terminal strands of the capsid proteins have important implications for virion assembly. Several of the "connecting loops" and COOH-terminal strands form prominent radial projections which are the antigenic sites of the virion.*

In 1908, Landsteiner and Popper identified poliovirus as the etiological agent of poliomyelitis (*1*). Since then poliovirus has played a unique role in biology and medicine. Poliovirus was the first virus to be grown in cultured cells (*2*), an accomplishment that led to the development of a killed virus and a live attenuated vaccine (*3*), to the physical and chemical characterization of the virion and its assembly intermediates (*4*), and to characterization of the virus life cycle within the infected cell (*5*).

The genome structures and the RNA sequences of several strains have been determined (*6*). Upon transfection into animal cells, full-length complementary DNA (cDNA) copies of the viral genome yield infectious virus, permitting the genetic analysis and manipulation of the virus (*7, 8*). Recently, monoclonal antibodies (*9*) and synthetic peptide antigens (*10–12*) have been used to map the antigenic sites of the virion onto the amino acid sequences of the capsid proteins. As a result of these and other studies, poliovirus has become one of the best characterized viral pathogens.

Poliovirus is a member of the picornavirus family, which also includes foot and mouth disease virus, hepatitis A virus, the rhinoviruses, and the coxsackie viruses. Poliovirus is approximately 310 Å in diameter with a molecular mass of 8.5×10^6 daltons (*4*). The virion is composed of 60 copies each of four coat-protein subunits—VP1 (306 amino acids, ~ 33 kD), VP2 (272 amino acids, ~30 kD), VP3 (238 amino acids, ~26 kD), and VP4 (69 amino acids, ~7.5 kD), and a single-stranded, plus-sense RNA genome of approximately 7500 nucleotides (*6*). The RNA is polyadenylated at its 3′ end (*4–8*) and is covalently linked at the 5′ end to the 22-amino-acid protein VPg (*13*).

The RNA contains a single large open-reading frame from which a 220 kD polyprotein is synthesized (*5, 6*). All known viral proteins are generated from this polyprotein in a cascade of proteolytic cleavages by virally encoded proteases (*14*). The capsid protein sequences are located at the NH_2-terminus of the polyprotein in the order VP4-VP2-VP3-VP1 (*6*). Early in the cascade, the capsid precursor P1-1a (*15*) is cleaved from the polyprotein. Subsequent cleavage of the P1-1a protomer (*16*) to VP0-VP3-VP1 is coupled with virion assembly. The final step in virion maturation is the cleavage of VP0, yielding VP4 and VP2 (*4*).

The three-dimensional structures of several intact plant viruses have been determined by x-ray crystallographic methods, including tomato bushy stunt virus (TBSV) (*17*), southern bean mosaic virus (SBMV) (*18*), and satellite tobacco necrosis virus (STNV) (*19*). Analyses of these structures have provided insight into the architecture and assembly of small spherical viruses. These studies have also provided a background of methodology and structural principles for the crystallographic investigation of animal viruses, for which the biology has been better characterized. We report here the structure of the Mahoney strain of type 1 poliovirus as determined by x-ray crystallographic methods; this structure provides a three-dimensional context for studying the relationship between the structure of an animal virus and its biological properties.

Crystallization and structure determination. Seed stocks of poliovirus type 1 (Mahoney strain) were obtained from an isolated plaque produced by transfection of HeLa cells with an infectious cDNA clone of the viral genome (*7*). The virus was propagated in HeLa cells, purified by standard methods (*20*), and crystallized by microdialysis at neutral *p*H (*21*). Virus recovered from redissolved crystals is fully infectious (*22*). The crystals belong to the orthorhombic space group $P2_12_12$ with $a = 322.9$, $b = 358.0$, and $c = 380.2$ Å and contain one-half virus particle per asymmetric unit. The particle center is located on the crystallographic twofold axis at approximately $Z = 0.25$ (*21, 23*). Three dimensional x-ray diffraction data for native crystals and for a platinum derivative (prepared by soaking crystals in 5 m*M* K_2PtCl_4 for 48 hours) were collected by oscillation photography to 2.9 Å resolution. Because the crystals were extremely sensitive to x-irradiation, the data were collected at −15°C, with 25 percent ethylene glycol as a cryosolvent. The photographs were digitized on a 50-μm raster with an Optronics P-1000 scanner and integrated and processed with the use of locally developed software (*24*). These and all subsequent calculations described below were carried out on a VAX 11/750 computer with 8 megabytes of memory and a 500-megabyte disk. Statistics for the native and derivative data are shown in Table 1.

The orientation of the poliovirus particle about the crystallographic twofold

J. M. Hogle and D. J. Filman are in the Department of Molecular Biology, Research Institute of Scripps Clinic, La Jolla, California 92037. M. Chow is in the Department of Applied Biological Sciences, Massachusetts Institute of Technology, Cambridge, and The Whitehead Institute for Biomedical Research, Cambridge, Massachusetts 02139.

axis was determined by evaluation of a one-dimensional icosahedrally locked rotation function, and the position of the particle along the twofold axis was estimated by inspection of native Patterson maps. Platinum substitution sites in the derivative crystals were determined by an icosahedrally locked Patterson vector search. One general and one fivefold axial platinum site were found per icosahedral asymmetric unit. Single isomorphous replacement (SIR) centroid phases were applied to the native amplitudes between 50 and 5 Å resolution. Native phases were refined at 5 Å resolution by iterative electron density averaging about the icosahedral symmetry elements as described by Bricogne (*25*). Several times during this phase refinement, the particle position and orientation, and the platinum substitution sites in the particle were optimized, treating them as variables in a systematic search which maximized the electron density at the predicted heavy atom sites in unaveraged derivative difference Fourier maps. After the final application of SIR phases, phase refinement at 5 Å converged in eight cycles; but the progress of the refinement suggested that SIR phases would be of limited use at higher resolution.

The structure determination was extended from 5 Å to 2.9 Å resolution by the addition of 0.05 Å shells of structure factor amplitudes in each cycle of density averaging. The new terms were phased by inversion of the previous cycle's averaged electron density. Similar methods have been used for phase extension in the structure determinations of STNV (*19*) and hemocyanin (*26*).

Alpha carbon positions were determined for all four capsid proteins, and correlated with the known amino acid sequence, in 3.6 Å averaged electron density maps. Phase extension and refinement were subsequently continued to 2.9 Å resolution. The complete process of extending phases between 5 and 2.9 Å resolution required 67 cycles of density averaging, yielding a quadratic R value of 0.27 and a correlation coefficient of 0.84 (*27*). Representative sections of the final 2.9 Å electron density map are shown in Fig. 1. Residue placement and side-chain identifications have been confirmed by inspection of this map. A full atomic model to fit the 2.9 Å map has not yet been completed.

Capsid protein subunits. The quality of the electron density map was such that it was possible to locate and identify almost all of the residues in all four capsid protein subunits. However, no electron density was present for residues 1 to 20 at the NH_2-terminus of VP1, residues 1 to 7 at the NH_2-terminus of VP2, residues 1 to 12 at the NH_2-terminus of VP4 (all of which are in the interior of the particle) and residues 234 to 238 at the COOH-terminus of VP3 (on the outside surface of the virion). In addition, there was no significant unassigned density that could correspond to the viral RNA or to VPg. The lack of density for the NH_2-terminal residues and the RNA implies that the interior of the virion is spatially disordered with respect to the icosahedrally symmetric protein shell.

The structures of VP1, VP2, and VP3 (Fig. 2) are remarkably similar to one another and surprising similar to the coat proteins of TBSV, SBMV, and STNV.

Table 1. Summary of the Mahoney native and platinum derivative data.

Items	Mahoney native	Pt derivative
Films (No.)*	120	37
Measurements (No.)	3,573,325	1,103,477
Unique *hkl* measured† (No.)	893,887	539,636
Selection criterion‡ (%)	50+	40+
Unique *hkl* used§ (No.)	736,926	310,063
R_{sym} versus mean‖	0.182	0.226
R_{sym} versus averaged whole¶	0.141	0.092

*The 0.5-degree oscillation photographs were taken on CEA reflex 25 film with Supper oscillation or with oscillation-precession cameras, with CuKα radiation from a Marconi GX-20 or GX-18 rotating anode generator with a 100-μm focus, and Franks mirror optics (*34*). Exposure times were 12 to 18 hours with the GX-20, and 6 to 8 hours with the GX-18. †Out of 950,000 unique reflections in the 2.9 Å sphere. ‡Partially observed reflections were corrected to their fully recorded equivalent by the method of Winkler, Schutt, and Harrison (*35*). Partials observed to an extent less than the indicated percentage were not used in constructing the unique data set. §A conservative cut based on the intensity and its standard deviation was used to exclude poorly measured reflections. ‖R_{sym} compares multiply measured individual corrected intensities (I_{hj}) with their sigma-weighted mean $\langle I_h \rangle$.

$$R_{sym} = \sum_h \sum_j | I_{hj} - \langle I_h \rangle | / \sum_h \sum_j \langle I_h \rangle$$

¶Same as (‖), with $\langle I_h \rangle$ computed with the use of fully recorded reflections only.

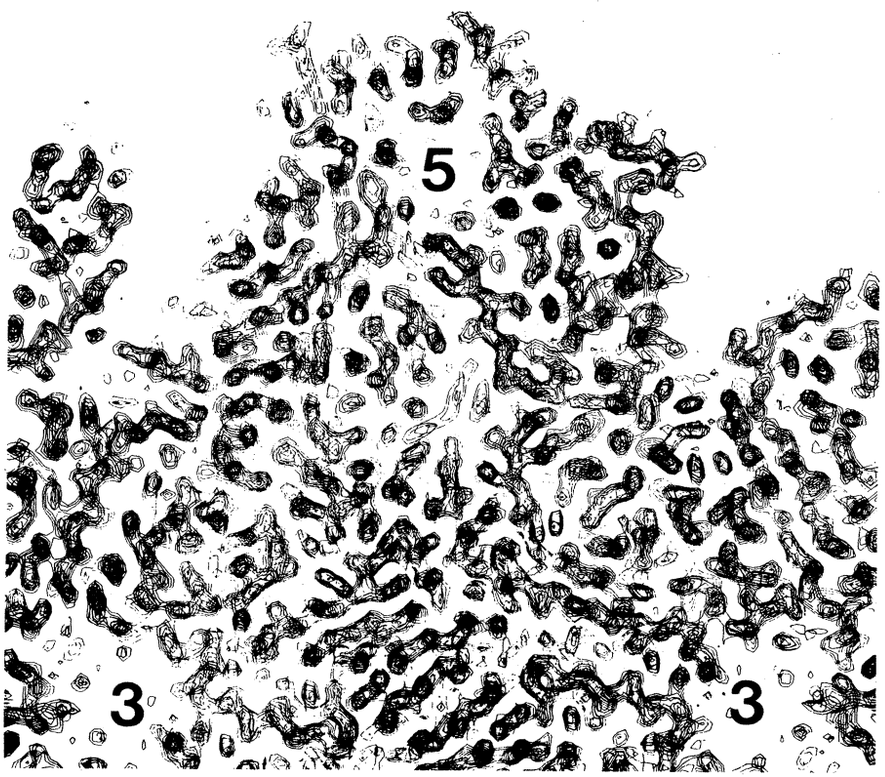

Fig. 1. Five representative sections of the final 2.9 Å averaged electron density map. The map encloses the icosahedral asymmetric unit of the poliovirion, sectioned perpendicular to the particle twofold axis. Sections from 120 to 124 Å are shown. Labels indicate the approximate positions of one fivefold and two threefold axes (which are skewed relative to the plane of the map). In this map, the connectivity of the main chain is unambiguous, the side chains are apparent, and there is partially resolved electron density for carbonyl oxygens. The quality of the map is also indicated by the level of noise at the protein-solvent interfaces. The lack of density at the top of the photograph is the result of solvent flattening.

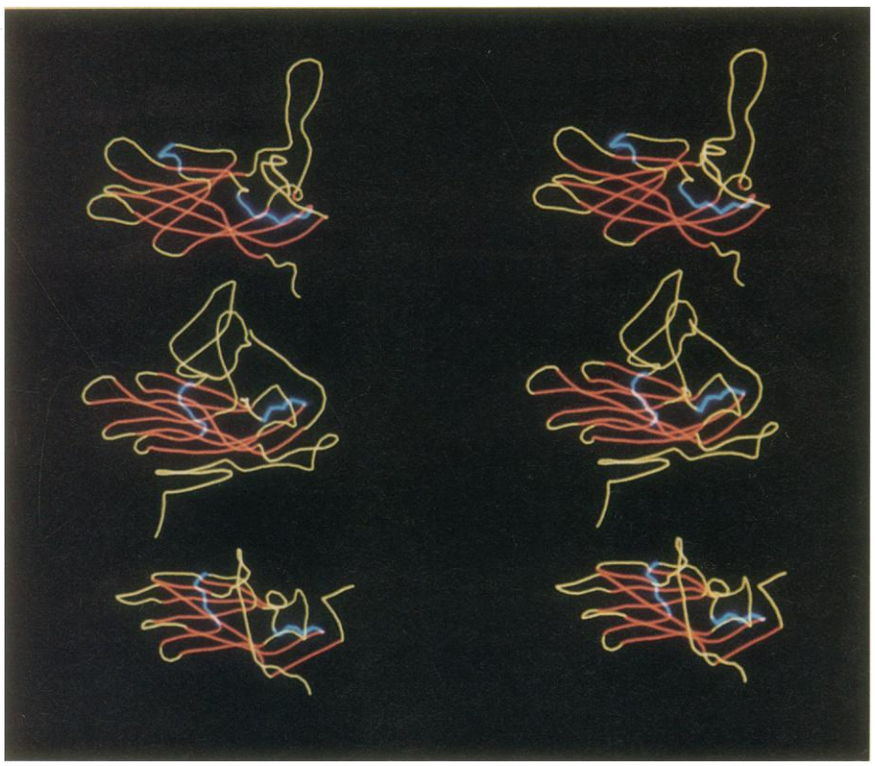

Fig. 2. Stereo picture of alpha carbon models of the poliovirus capsid proteins (*36*): VP1 (top), VP2 (middle), VP3 (bottom). Portions of the main chain corresponding to the eight-stranded antiparallel beta barrel are red; the conserved flanking helices are blue; variable internal loops and terminal extensions are yellow. The NH_2- and COOH-terminal extensions of VP1 and the NH_2-terminal extension of VP3 have been truncated for clarity.

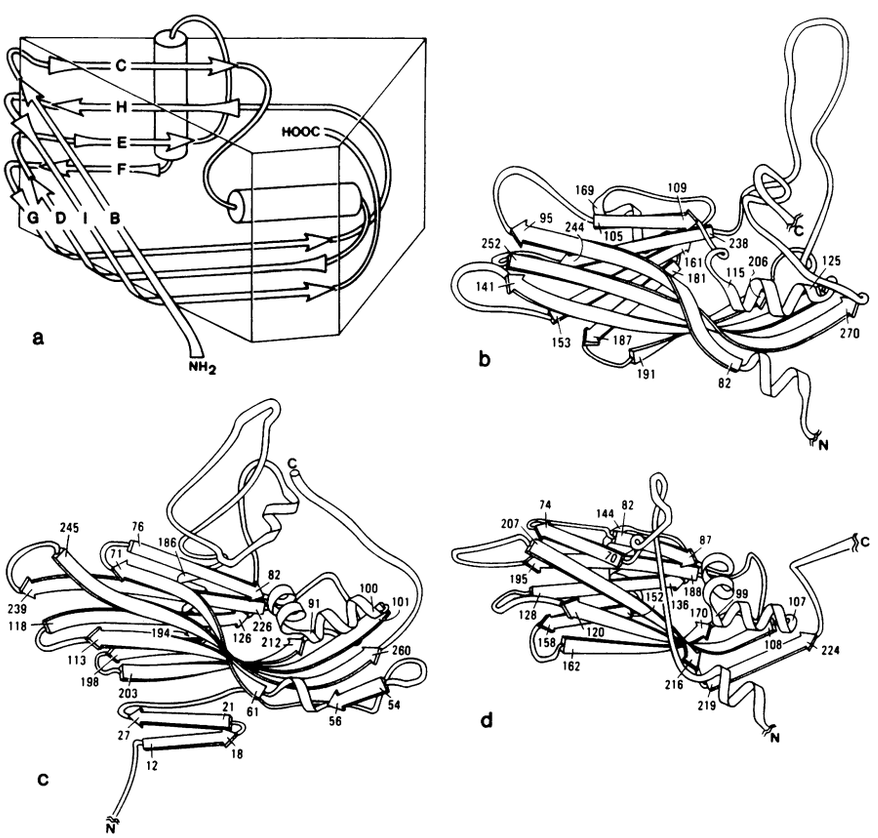

Fig. 3. Schematic representation of the poliovirus capsid proteins. (a) Simplified diagram showing the topology of the structurally conserved "core." Beta strand designations are consistent with those used to describe the capsid proteins of the plant viruses (*38*). Ribbon diagrams show (b) VP1, (c) VP2, and (d) VP3. The NH_2- and COOH-terminal extensions of VP1 and the NH_2-terminal extension of VP3 have been truncated for clarity.

Each of these proteins consists of a "core," or common structural motif, with variable "elaborations." The cores are topologically identical. Each core is composed of an eight-stranded antiparallel beta barrel with two flanking helices. Four strands (B, I, D, and G in Fig. 3a) make up a large twisted beta sheet which forms the front and bottom surfaces of the barrels (Fig. 3, b to d). The remaining four strands (C, H, E, and F) make up a smaller, flatter beta sheet which forms the back surface of the barrel. The strands comprising the front and back surfaces are joined at one end by four short loops, giving the barrel the shape of a triangular wedge. In poliovirus, each of the three coat proteins has different NH_2- and COOH-terminal extensions, and includes a different set of internal insertions. The largest internal insertion in VP1 (residues 207 to 237) is the loop connecting beta strands G and H. The largest insertion in VP2 (residues 127 to 185) connects beta strand E with the radial helix on the back surface of the barrel. The most significant excursion in VP3 (residues 53 to 69) connects the NH_2-terminal strand to beta strand B. The NH_2-terminal strands of VP1, VP2, and VP3 fold beneath the barrels, while the internal insertions and COOH-terminal additions are located on the top surface of the barrel.

In contrast to the compact structures found in the other three coat proteins, VP4 has a more extended conformation. The only significant compact structure in VP4 is a short two-stranded antiparallel beta sheet near its NH_2-terminus. VP4 is similar in its position and conformation to the NH_2-terminal strands of VP1 and VP3, and thus it appears to function as the (detached) NH_2-terminal extension of VP2 rather than as an independent capsid protein.

Protomer subunit. The position and orientation of the four capsid proteins on the icosahedral surface of the virion are shown in Fig. 4. The closed end of the barrel of VP1 is located near the fivefold axis. The closed ends of the VP2 and VP3 barrels alternate around the particle threefold axis. The subunits shown are those that have the most extensive intersubunit interactions, and thus they are likely to be the ones that are derived by cleavage of the same P1-1a protomer. On the outer surface of the particle, the COOH-terminus of VP1 wraps over VP3, while residues 207 to 237 and 271 to 295 of VP1 flank the outer surface of VP2 (Fig. 4, center). On the inner surface, the interactions are more extensive. The NH_2-terminal strand of VP3 wraps around the base of the VP1 barrel, while

the NH_2-terminal strand of VP1 makes extensive contacts with the inner surface of the VP3 barrel (Fig. 4, bottom).

Outer surface of the virion. The continuous protein shell of the poliovirion extends from approximately 110 to 140 Å radius (Fig. 5a). The exterior surface of the virion (Fig. 5, b and c) is dominated by two sets of prominent radial extensions: A ribbed peak (extending to 165 Å radius) is formed at the fivefold axes by residues from VP1, and a broad plateau is formed at the threefold axes by residues from VP2 and VP3. The plateau extends to 150 Å radius at its center, and is ringed by promontories. The peaks at the fivefold axes are surrounded by broad valleys, while adjacent plateaus are separated by saddle surfaces at the particle twofold axes. Thus, the exterior surface of the poliovirus particle is approximated by the geometric construction shown in Fig. 6a. This construction appears in the other figures to aid in orientation.

VP1, VP2, and VP3 occupy sites in the poliovirus capsid that are analogous to those of the A, C, and B subunits, respectively, in the $T = 3$ plant viruses. However, the external surface of poliovirus differs significantly from those of SBMV and of the S domain of TBSV. In the $T = 3$ plant viruses, the upper surfaces of the cores of the three capsid proteins in one icosahedral asymmetric unit, and the three in a twofold related icosahedral asymmetric unit are coplanar, forming the face of a rhombic triacontahedron (Fig. 6b). The greater relief of the poliovirion surface can be ascribed to differences in the packing and orientation of the capsid protein subunits.

A pronounced tilt of the closed end of the VP1 barrel outward along the fivefold axis is responsible for the prominent

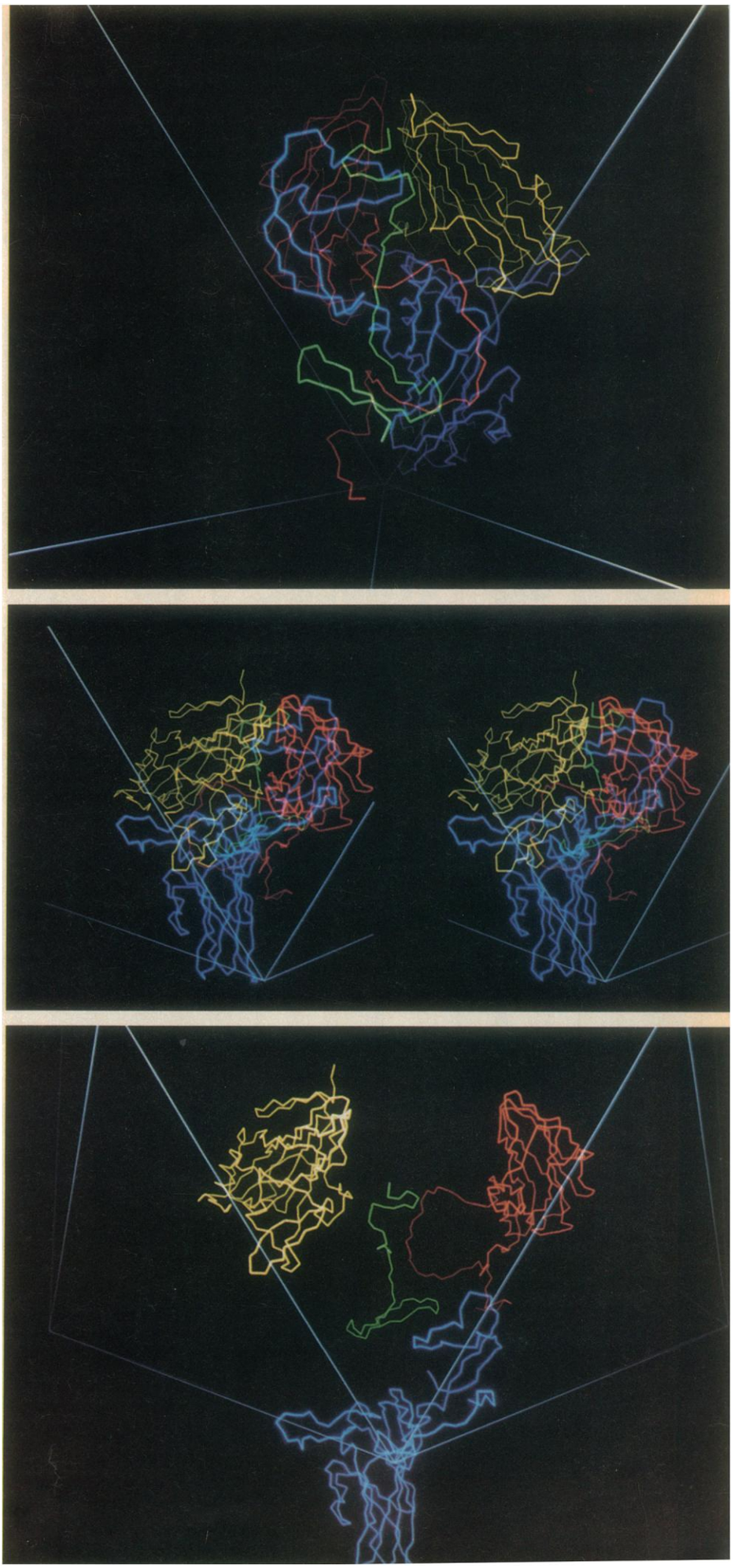

Fig. 4. Alpha carbon models of the four poliovirus capsid proteins which constitute a protomer (derived by cleavage of a single molecule of the P1–1a precursor) (*36*). VP1 is blue, VP2 is yellow, VP3 is red, VP4 is green. Portions of the structure close to the view point are brighter than portions which are further away. The edges of an icosahedron are included to indicate the orientation of the protomer relative to the icosahedral symmetry elements of the virus particle. (Top) An "exploded" view of the capsid proteins, showing the relationships of VP4 and the terminal extensions of VP1 and VP3 to the major compact domains of the capsid proteins. (Center) Stereo picture of the protomer, viewed from the outside of the virion. VP1 is adjacent to the fivefold axis. VP2 and VP3 alternate around particle threefold axes. (Bottom) View of the protomer from the inside of the virion. This view is heavily depth-cued to emphasize VP4 and the NH_2-terminal extensions of VP1 and VP3.

fivefold peaks (Fig. 7, a and b). The upper surface of the VP1 barrel forms the slope of the peak, and the uppermost three loops of the barrel (residues 96 to 104, 245 to 251, and 142 to 152) are exposed at the summit. The top loop (96 to 104) twists out from the surface of the subunit so that it is particularly well exposed, giving the fivefold peak a ribbed appearance. Indeed, this loop contains the only trypsin-sensitive site in the Sabin strain of type 1, and the Sabin and Leon strains of type 3 poliovirus (*28*).

The outward tilt of the closed ends of the VP2 and VP3 barrels along the threefold axes is less pronounced. As a result, only the outermost two loops (residues 72 to 75 and 240 to 244 in VP2, and residues 75 to 81 and 196 to 206 in VP3) are exposed. The plateau at the threefold axis is broadened by two sets of outward projections. The smaller projection, which extends to a radius of 155 Å, is formed by the insertion in the B strand of VP3 (residues 53 to 69). The larger projection, which extends to 165 Å radius, is formed by the internal insertion in VP2 (residues 127 to 185), and is supported at its base by the COOH-terminal strand of VP2 (residues 261 to 272), and by residues 207 to 237 and 271 to 295 from VP1.

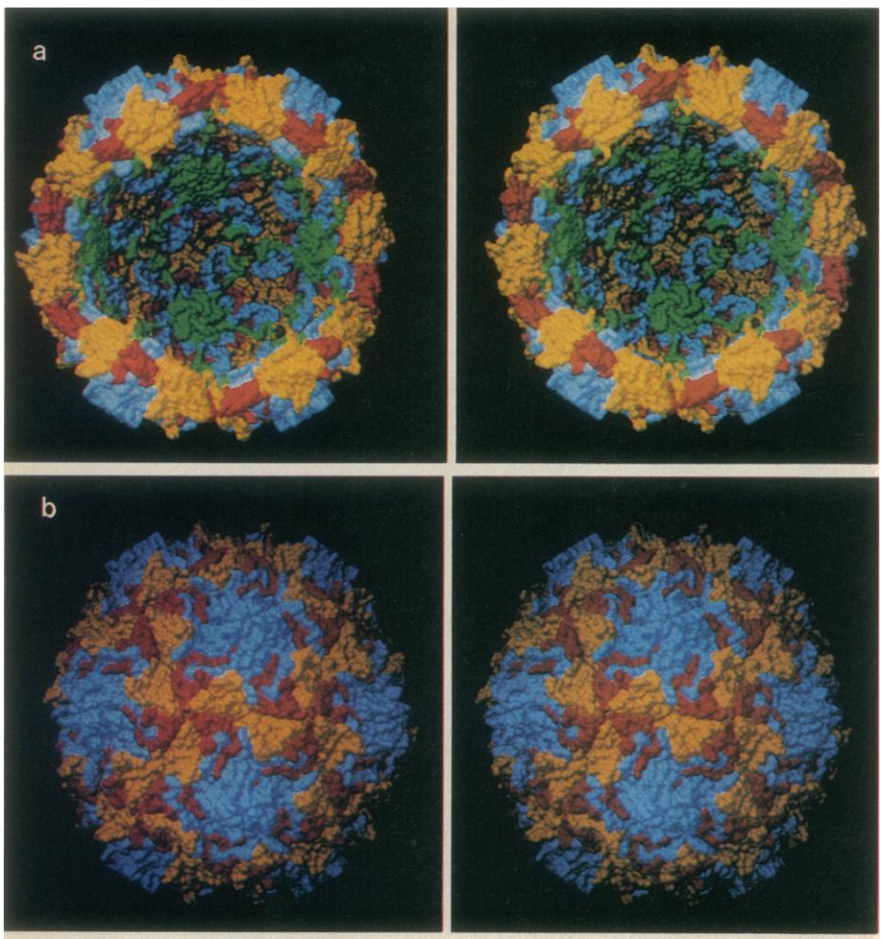

Fig. 5. Major features on the surface of poliovirus. VP1 is blue, VP2 is yellow, VP3 is red, VP4 is green. (a) Stereo space-filling representation of the interior surface (*37*). Four pentamers have been removed from the capsid shell. The thickness of the shell and the volume of the cavity occupied by RNA are apparent. (b) Stereo space-filling representation of the exterior surface (*37*). (c) Packing of eight protomers on the exterior surface of poliovirus (*36*). The symmetry elements of the particle are indicated by the edges of an icosahedron and a dodecahedron (as described in the legend of Fig. 6). Portions of the structure close to the view point are brighter than portions which are further away. In (b) and (c), note the ribbed peak formed by VP1; the broad plateau ringed by promontories formed by VP2 and VP3; the broad valley surrounding the fivefold peak; and the saddle surface across the twofold axis.

Subunit packing. In the $T = 3$ plant viruses, the three subunits in each icosahedral asymmetric unit (as defined in Fig. 6b) are related by a local threefold axis. Within the asymmetric unit, the pairwise contacts between the A and B, B and C, and C and A subunits are nearly identical. In addition, the contact between fivefold related A subunits is nearly identical to one of the two distinct types of interaction between B and C subunits at the threefold axes (*17, 18*). These similarities reflect the constraints imposed by quasi-equivalent packing of chemically identical subunits (*29*).

In poliovirus, VP1, VP2, and VP3 are chemically distinct, so the constraints are relaxed. The relaxation of constraints permits qualitative differences in the "tilts" of the subunits (as described above), causing significant differences in the contacts between subunits. Two specific examples serve to demonstrate these differences. (i) The "tangential" helices of VP1 and VP3 (shown in the front of Fig. 3a) are packed against one another at approximately a 45-degree angle. In contrast, the analogous packing of helices between twofold related molecules of VP2 resembles that in the $T = 3$ plant viruses, wherein the helix axes are nearly parallel. (ii) In VP2, VP3, and in the A, B, and C subunits of the $T = 3$ plant viruses, the loop that connects beta strand E to the "radial" helix (shown in the back of Fig. 3a) lies in the interface between subunits within the triangular icosahedral asymmetric unit defined in Fig. 6b. In contrast, the analogous loop of VP1 does not lie in the VP1–VP3 interface. As a result of the pronounced tilt of VP1, the loop is entirely exposed on the surface of the virion. These differences in subunit contacts indicate that the packing of VP1 cores around the fivefold axes is dissimilar from the packing of VP2 and VP3 around the threefold axes. They also demonstrate that, unlike the $T = 3$ plant viruses, there is no satisfactory local threefold axis relating the subunits within an icosahedral asymmetric unit.

Inner surface of virion. The interior

surface of the capsid is formed by the bottom surfaces of the beta barrels of VP1, VP2, and VP3, by VP4, and by the NH_2-terminal strands of VP1, VP2, and VP3. The NH_2-termini form an extensive network (Fig. 7c) which links fivefold related protomers together to form pentamers; twofold related pentamers are also linked by this network, though less strongly. The most striking feature of the inner surface is the interaction between the NH_2-termini of VP3 and VP4 about the fivefold axis (Fig. 7, c and d). The NH_2-termini of five subunits of VP3 intertwine about the fivefold axis forming a five-stranded tube of extremely twisted parallel beta structure. This twisted tube is flanked on its lower surface by five two-stranded antiparallel beta sheets from the NH_2-termini of VP4. A structure analogous to the twisted tube, described as a "beta annulus," occurs at the threefold axes of the $T = 3$ plant viruses (*17, 18*).

Implications for assembly. The extensive network of interactions between fivefold related protomers is consistent with earlier proposals that the pentameric association of VP0, VP3, and VP1 is an intermediate in the assembly of poliovirions (*4*). In particular, the twisted tube formed around fivefold axes by the NH_2-termini of VP3 is a structure that can form only upon pentamer assembly. This structure may direct pentamer formation and is expected to contribute substantially to the stability of the pentamers once formed. The role of the NH_2-terminal network in poliovirus differs from that of an analogous network in the $T = 3$ plant viruses, wherein the "arms" which are linked at the threefold "beta annuli" form a $T = 1$ scaffold which determines local curvature and thereby directs assembly of the $T = 3$ capsid (*30*).

The cleavage of VP0, yielding VP4 and VP2, is believed to be the final step in virion maturation, occurring after capsid assembly and the encapsidation of RNA (*4*). The COOH-terminus of VP4 and the NH_2-terminus of VP2 are close to one another in the interior of the mature virion. Unless there is a substantial rearrangement of the capsid structure after the cleavage of VP0, the cleavage site is inaccessible to external proteases. Consequently, the cleavage of VP0 may be autocatalytic. The internal position of VP4 also suggests that the loss of this protein upon inactivation of the virus at elevated temperatures (55° to 60°C) or upon cell attachment (*4*) signifies a substantial rearrangement of the virion structure.

One remarkable discovery resulting from the structure determination is that the NH_2- and COOH-termini generated by proteolytic processing of P1-1a to VP0, VP3, and VP1 are spatially distant, and indeed, are located on opposite surfaces of the pentamer. The separation of these termini and the extensive interaction of the NH_2-terminal strands of VP3 about the fivefold axes are most consistent with a proposed assembly pathway (*4*) in which the cleavage of P1-1a occurs prior to pentamer formation. Processing of P1-1a after pentamer formation would require far more elaborate conformational changes. In either case, substantial structural rearrangements must occur subsequent to proteolytic cleavage. This confirms the proposal (*4*) that posttranslational processing plays a significant role in controlling virion assembly.

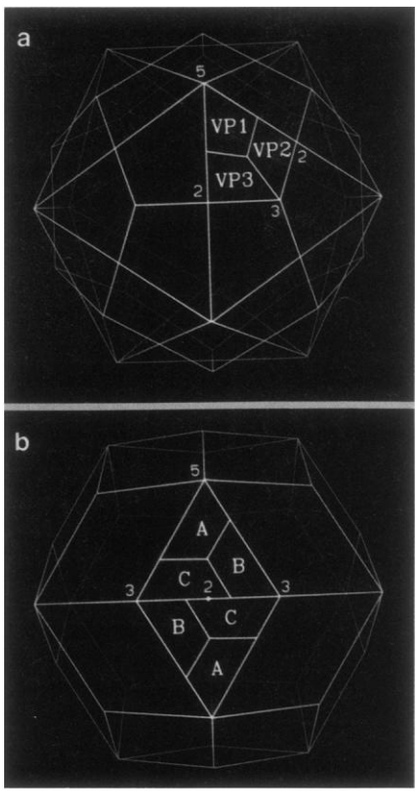

Fig. 6. Geometric representations of the exterior surface features of poliovirus and of the $T = 3$ plant viruses. (a) In this construction, the edges of an icosahedron and a dodecahedron intersect along twofold axes. The resulting surface resembles poliovirus in that it has somewhat larger prominences at its fivefold axes than at its threefold axes. Labels indicate the positions of VP1, VP2, and VP3 from the same protomer. Each protomer occupies an icosahedral asymmetric unit bounded by one fivefold, one threefold, and two twofold axes. (b) A rhombic triacontahedron: a simplified representation of the surface of southern bean mosaic virus (*18*), and tomato bushy stunt virus (*17*). Labels indicate the positions of the six capsid subunits that are contained in two icosahedral asymmetric units. The A, C, and B subunits of the $T = 3$ plant viruses lie in positions analogous to those of the poliovirus subunits VP1, VP2, and VP3, respectively.

Sequence differences between strains and serotypes. Sequence differences between naturally occurring strains of influenza virus have been used to identify several distinct sites on the hemagglutinin (*31*) and neuraminidase (*32*) which are responsible for antigenic drift. The success of this approach may be attributed to the availability of several strains which were derived from one another in a known temporal sequence under immune selection. In poliovirus, however, the evolutionary relationships between the three serotypes are unknown, and the role of immune selection in the emergence of new field isolates is unclear. As a result, specific sequence differences in the existing strains cannot be ascribed to immune selection with any confidence.

Differences in the amino acid sequences of the capsid proteins of type 1 Mahoney and type 3 Leon strains were mapped onto the Mahoney structure. The sequence differences were distributed widely over the inner and outer surfaces of the capsid proteins, but were conspicuously absent from the cores of the subunits. This distribution shows that, notwithstanding the selective pressures for change, the inherent constraints imposed by protein folding and assembly exert a strong selective pressure for sequence conservation.

Location of neutralizing antigenic determinants. A more direct procedure for determining antigenic sites is the use of neutralizing antiviral monoclonal antibodies to select for mutant viruses resistant to neutralization (*9*). The locations of sequence changes that confer such resistance are shown in Fig. 7e. The mutation sites map onto the major external surface features of the virion. These "escape mutations" can be grouped on the basis of proximity into four discrete clusters (Fig. 7, e and f). Cluster 1 (colored yellow) contains residues from the loops of VP1 which form the fivefold peak, as well as nearby residues from the loop (162 to 178) that lies along the upper surface of the VP1 barrel. Cluster 2 (blue) includes residues from the internal insertion in VP3 and from the top loop of the barrel in VP2. Cluster 3 (green) is formed by residues from the internal insertion in VP1, the internal insertion in VP2, and the COOH-terminus of VP2. The grouping of these three segments into one antigenic cluster by proximity is confirmed by the observation that a mutation in the insertion of either VP1 or VP2 conferred resistance to the same

neutralizing monoclonal antibody (*33*). Cluster 4 (red) contains residues from a loop (271 to 295) in the COOH-terminal strand of VP1. Although this site has been identified as a distinct cluster, it is sufficiently close to clusters 2 and 3 that it might become continuous with either one when a larger number of viral mutants are identified. One unexplained observation is that most of the escape mutations in the Mahoney and Sabin strains of type 1 poliovirus occur in clusters 2 and 3, whereas nearly all of the escape mutations in the Leon and Sabin strains of type 3 poliovirus are located in cluster 1, in residues 90 to 103 of VP1. Nonetheless, all of the mutation sites occur in exposed loops on the surface of the virion which are readily accessible to antibody binding. Thus, it is unnecessary to propose that any of these mutations allow the virus to escape neutralization by acting at a site which is distant from the antibody binding site.

Synthetic peptide immunogens have also been used to identify the antigenic sites of poliovirus (*10–12*). A number of these peptides have been shown to induce antibodies that bind or neutralize virions (or both); or alternatively, to prime animals for a neutralizing response to a subsequent subimmunizing dose of virions. With the exception of several peptides from VP1, the immunogenic peptides correspond to sequences that are located on the outer surface of the

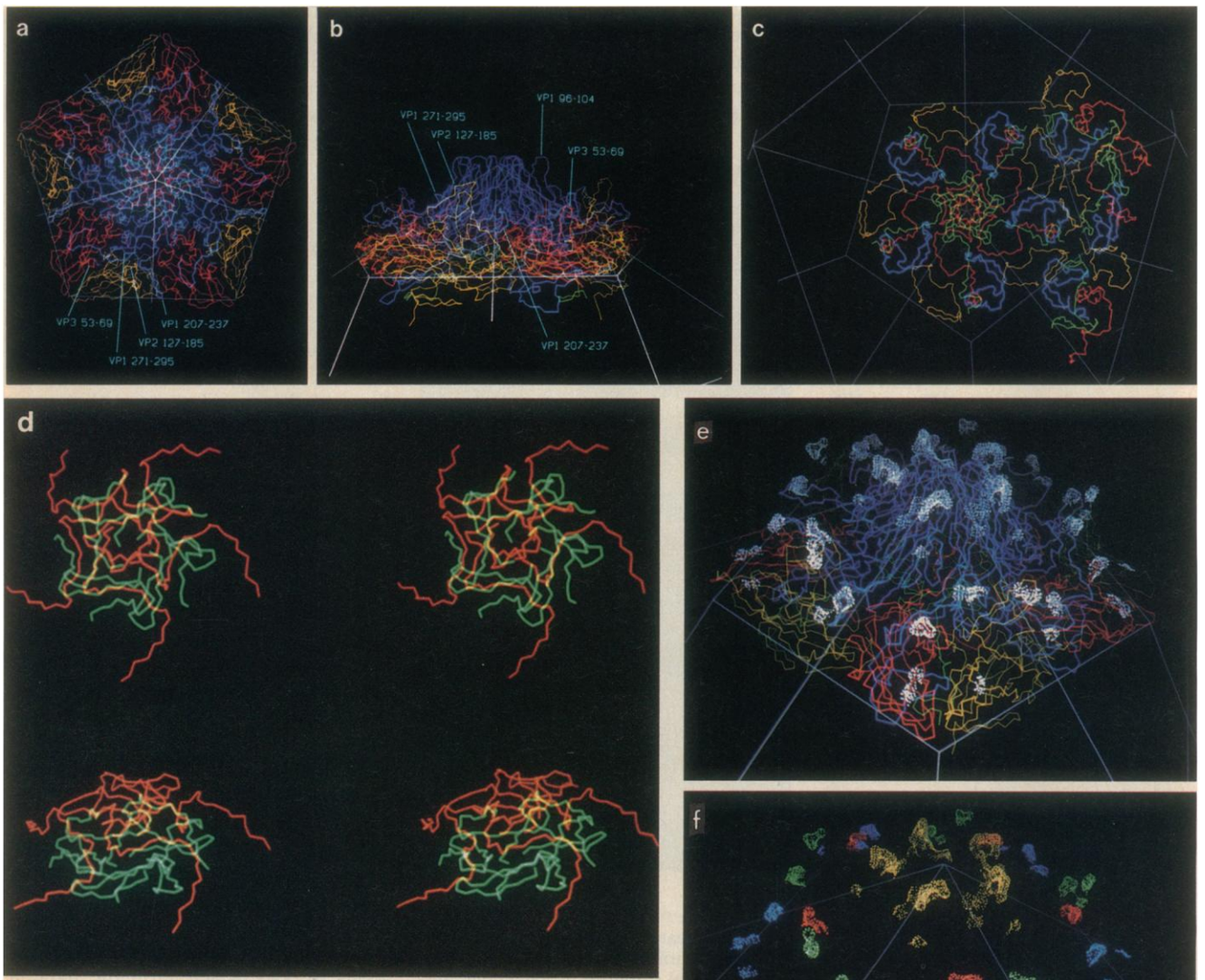

Fig. 7. Selected views of portions of the poliovirus structure (*36*). VP1 is blue, VP2 is yellow, VP3 is red, VP4 is green. Portions of the structure close to the view point are brighter than portions which are further away. The edges of an icosahedron and a dodecahedron (as described in Fig. 6) are included as an orientation aid. (a) The outer surface of five VP1-VP2-VP3-VP4 protomers, viewed along the fivefold axis. Loops discussed in the text are labeled by residue number. (b) Side view of the same pentamer shown in (a). (c) Network formed by VP4 and the NH_2-terminal extensions of VP1, VP2, and VP3, viewed from the inside of the virus particle. The remainder of the capsid protein molecules have been omitted for clarity. Strands from eight protomers are depicted. (d) Stereo pictures showing the structure formed around the fivefold axis by the interaction of five copies each of VP4 and the NH_2-termini of VP3. The structure is located on the interior surface of the capsid. Top: the view along the fivefold axis looking toward the particle center. Bottom: side view. (e) Dot surfaces indicate the positions of monoclonal release mutations on the virion outer surface. (f) Dot surfaces have been color-coded to indicate clusters of monoclonal release mutations grouped by proximity. Clusters 1, 2, 3, and 4 (as defined in the text) are colored yellow, blue, green, and red, respectively. Dot surfaces in (e) and (f) were computed using a 3 Å probe sphere and the alpha carbon model. Only residues corresponding to monoclonal release mutations are highlighted.

virion, within the clusters of antibody-induced mutation sites. One exception is the peptide corresponding to residues 113 to 121 of VP1 (*12*). The NH_2-terminal portion of this peptide is partially exposed and lies close to cluster 4, so that it may represent an extension of this cluster. The other exceptions are peptides from the NH_2-terminal strand of VP1 or from the bottom loop of VP1 (residues 182 to 201), all of which are deeply buried in the interior of the virion. Two of these peptides (61 to 80 and 182 to 201) induce a significant (1:150 to 1:200) neutralizing response in both rabbits and rats (*10*). The ability of these buried peptides to induce an antiviral response may prove to be important in understanding the mechanism of neutralization.

In conclusion, the crystal structure of poliovirus has yielded important insights into the structure and assembly of small spherical viruses. In addition, the structure furnishes a three-dimensional framework for studying properties that are especially relevant to animal viruses. The mapping of monoclonal release mutants and of peptides that induce neutralizing antibodies to virus has produced a detailed description of the distribution of antigenic sites on an intact virus. This information is expected to lead to an understanding of the mechanism of neutralization. We also anticipate that the structure will be useful for the design and interpretation of experiments in other areas of biological and medical importance, such as the role of capsid structure in host- and tissue-specificity, and in the attenuation of neurovirulence. Thus, the poliovirus structure provides an excellent opportunity to study viral pathogenesis at the molecular level.

References and Notes

1. K. Landsteiner and E. Popper, *Wien. Klin. Wochenshr.* **21**, 1830 (1908).
2. J. F. Enders, T. H. Weller, F. C. Robbins, *Science* **109**, 85 (1949).
3. J. Salk and D. Salk, *ibid.* **195**, 837 (1977); A. B. Sabin and C. R. Boulger, *J. Biol. Stand.* **1**, 115 (1973).
4. As reviewed by: R. R. Rueckert, in *Comprehensive Virology*, H. Fraenkel-Conrat and R. Wagner, Eds. (Plenum, New York, 1976), vol. 6, pp. 131–213; J. R. Putnak and B. A. Phillips, *Microbiol. Rev.* **45**, 287 (1981).
5. As reviewed by L. Levintow, in *Comprehensive Virology*, H. Fraenkel-Conrat and R. Wagner, Eds. (Plenum, New York, 1974), vol. 2, pp. 109–171.
6. N. Kitamura *et al.*, *Nature (London)* **291**, 547 (1981); V. Racaniello and D. Baltimore, *Proc. Natl. Acad. Sci. U.S.A.* **78**, 4887 (1981); G. Stanway *et al.*, *Nucleic Acids Res.* **11**, 5629 (1983); G. Stanway *et al.*, *Proc. Natl. Acad. Sci. U.S.A.* **81**, 1539 (1984); H. Toyoda *et al.*, *J. Mol. Biol.* **174**, 561 (1984).
7. V. Racaniello and D. Baltimore, *Science* **214**, 916 (1981).
8. B. L. Semler, A. J. Dorner, E. Wimmer, *Nucleic Acids Res.* **12**, 5123 (1984); T. Omata *et al.*, *Gene* **32**, 1 (1984).
9. E. A. Emini, B. A. Jameson, A. J. Lewis, G. R. Larsen, E. A. Wimmer, *J. Virol.* **43**, 997 (1982); R. Crainic *et al.*, *Infect. Immun.* **41**, 1217 (1983); P. Minor *et al.*, *Nature (London)* **301**, 674 (1983); P. Minor *et al.*, *J. Gen. Virol.* **65**, 1159 (1985); M. Ferguson *et al.*, *Virology* **143**, 505 (1985); D. C. Diamond *et al.*, *Science* **229**, 1090 (1985).
10. M. Chow, R. Yabrov, J. Bittle, J. Hogle, D. Baltimore, *Proc. Natl. Acad. Sci. U.S.A.* **82**, 910 (1985).
11. E. A. Emini, B. A. Jameson, E. Wimmer, *Nature (London)* **304**, 699 (1983); *J. Virol.* **52**, 719 (1984); in *Modern Approaches to Vaccines*, R. M. Channock and R. A. Lerner, Eds. (Cold Spring Harbor Laboratory, Cold Spring Harbor, N.Y., 1984), pp. 65–76; M. Ferguson *et al.*, *Virology* **143**, 505 (1985).
12. B. A. Jameson, J. Bonin, M. G. Murray, E. Wimmer, O. Kew, in *Vaccines 85*, R. Lerner, R. M. Channock, F. Brown, Eds. (Cold Spring Harbor Laboratory, Cold Spring Harbor, N.Y., 1985), pp. 191–198.
13. E. Wimmer, *Cell* **28**, 199 (1982).
14. M. A. Pallansch *et al.*, *J. Virol.* **49**, 873 (1984).
15. R. R. Rueckert and E. Wimmer, *ibid.* **50**, 957 (1984).
16. The term "protomer" will refer to a single molecule of P1–1a, or to a set of proteins derived from it by further proteolytic processing (VP0-VP3-VP1 or VP4-VP2-VP3-VP1).
17. S. C. Harrison, A. J. Olson, C. E. Schutt, F. K. Winkler, G. Bricogne, *Nature (London)* **276**, 368 (1978).
18. C. Abad-Zapatero *et al.*, *ibid.* **286**, 33 (1980).
19. L. Liljas *et al.*, *J. Mol. Biol.* **159**, 93 (1982).
20. D. Baltimore, M. Girard, J. E. Darnell, *Virology* **29**, 179 (1966); M. H. Baron and D. Baltimore, *Cell* **28**, 395 (1982).
21. J. M. Hogle, *J. Mol. Biol.* **160**, 663 (1982).
22. J. P. Icenogle and J. M. Hogle, unpublished data.
23. J. T. Finch and A. Klug, *Nature (London)* **183**, 1709 (1959).
24. D. J. Felman and J. M. Hogle, in preparation.
25. G. Bricogne, *Acta Crystallogr.* **A30**, 395 (1974); *ibid.* **A32**, 832 (1976).
26. W. P. J. Gaykema *et al.*, *Nature (London)* **309**, 23 (1984).
27. The quadratic R value and the linear correlation coefficient are measures of the agreement between two sets of structure factor amplitudes: those observed and those calculated by Fourier inversion of the averaged electron density map. The square of R is equal to the sum of the squares of the unweighted differences, divided by the sum of the observed reflection intensities.
28. C. E. Fricks, J. P. Icenogle, J. M. Hogle, *J. Virol.* **54**, 856 (1985).
29. D. L. D. Caspar and A. Klug, *Cold Spring Harbor Symp. Quant. Biol.* **27**, 1 (1962).
30. S. C. Harrison, *Biophysics J.* **32**, 139 (1980).
31. D. C. Wiley, I. A. Wilson, J. J. Skehel, *Nature (London)* **289**, 373 (1981).
32. P. M. Colman, J. N. Varghese and W. G. Laver, *ibid.* **305**, 41 (1983).
33. P. Minor, personal communication.
34. S. C. Harrison, *J. Appl. Cryst.* **1**, 84 (1968).
35. F. K. Winkler, C. E. Schutt, S. C. Harrison, *Acta Crystallogr.* **A35**, 901 (1979).
36. Color figures were produced by Dan Bloch using the graphics language GRAMPS [T. J. O'Donnell and A. J. Olson, *Comput. Graphics* **15**, 133 (1981)]. The molecular modeling program GRANNY [M. L. Connolly and A. J. Olson, *Comput. Chem.* **9**, 1 (1985)], and the molecular surface program MS [M. L. Connolly, *Science* **221**, 709 (1983)].
37. Space-filling representations were produced by A. J. Olson, using the molecular surface programs AMS [M. L. Connolly, *J. Appl. Crystallogr.* **16**, 548 (1983)] and RAMS [M. L. Connolly, *J. Mol. Graph.* **3**, 19 (1985)].
38. M. G. Rossmann *et al.*, *J. Mol. Biol.* **165**, 711 (1983).

39. Supported by NIH grant AI-20566 (J.M.H.), in part by a grant from the Rockefeller Foundation and by NIH grant AI-22346 to D. Baltimore (Whitehead Institute for Biomedical Research), and by NIH training grants NS-07078 and NS-12428 (D.J.F.). Preliminary crystallographic studies that led to this work were supported by NIH grant CA-13202 to S. C. Harrison. We thank R. Lerner, D. Baltimore, and S. C. Harrison for interest and support throughout various phases of this work; D. Bloch for assistance in the computer graphics, E. Getzoff for helping to prepare the ribbon diagrams in Fig. 3. A. J. Olson for preparing Fig. 5, a and b, and J. Icenogle, C. Fricks, M. Oldstone, and I. Wilson for comments and discussions. We also thank P. Minor for sharing his data on monoclonal release mutants prior to publication. This is publication No. MB4075 of the Research Institute of Scripps Clinic.

13 August 1985; accepted 30 August 1985